



The role of small separation interactions in ferrofluid structure

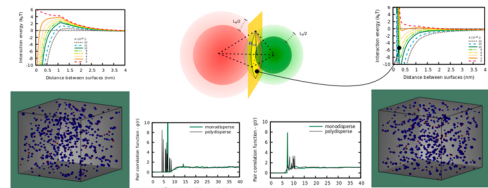
Leonardo Luiz e Castro ^{a,*}, Caio César Cavalcante Amorim ^a, João Pedro Valeriano Miranda ^b, Tiago de Sousa Araújo Cassiano ^a, Fábio Luís de Oliveira Paula ^a

^a Instituto de Física, Universidade de Brasília (UnB) – Campus Universitário Darcy Ribeiro, Brasília, DF 90919-900, Brazil

^b Instituto de Física Teórica, Universidade Estadual Paulista (UNESP) – R. Dr. Bento Teobaldo Ferraz, 271, Bloco 2, Barra-Fundão, São Paulo, SP 01140-070, Brazil



GRAPHICAL ABSTRACT



ARTICLE INFO

Keywords:
Ferrofluid
Magnetic colloid
DLVO
Monte Carlo
Van der Waals forces
EDL repulsion
Born-Mayer repulsion
Cohesion energy
Derjaguin approximation

ABSTRACT

Interparticle interactions in colloids are traditionally modeled by means of the DLVO theory, which includes van der Waals and electrical double layer (EDL) interactions. However, the validity range limitations become critical in biocompatible magnetic colloids, requiring a more detailed description of the interactions, especially at small intersurface separations. As magnetic colloids, ferrofluids require an extended DLVO (XDLVO) model that includes magnetic interactions. Moreover, the nanoparticles of biocompatible ferrofluids are usually ionic-surfacted, such that their charged surfactants interact both electrically and sterically. In some of such particles, the charge is usually not located at the surface, but at the outer extremities of the surfactant molecules, and this feature restricts the EDL model validity to larger separation distances. We addressed this problem by means of a model proposed by Schnitzer and Morozov, which employs a generalized Derjaguin approximation that makes the EDL repulsion expression valid for all separations. The van der Waals expression of the DLVO theory is also problematic because it shows an unphysical divergence as the intersurface separation tends to zero, a problem that was circumvented by replacing the expression at small separations with another expression based on cohesion energy and the Born-Mayer repulsion. The modifications proposed here are of interest for research on colloids in general and our Monte Carlo simulations show that they acquire even greater importance when it comes to ferrofluids. The influence of magnetic interparticle interactions on the colloid structure is better gauged using these modifications, which prevent magnetic interactions from being obfuscated by artificially large van der Waals and EDL interactions. This conclusion makes the small separation treatment particularly important for the study of magnetic colloids.

* Corresponding author.

E-mail address: llcastro@unb.br (L.L. e Castro).

1. Introduction

Ferrofluids were first described in a patent [1] as colloidal suspensions of magnetic particles. Since then, they have attracted extensive interest for the possibility of remote positioning and control by means of applied magnetic field [2], making them suitable for technological and biomedical applications [3–6]. Structurally, ferrofluids are colloidal dispersions of ferromagnetic nanoparticles in a liquid solvent.¹ The ferromagnetism of the nanoparticles and the fluidity of the solvent are combined to create the unique behavior of ferrofluids. Many ferrofluid applications require its stability as a fluid (colloidal stability), while presenting minimal viscosity variations, as they are frequently related to particle agglomeration and gel transition [2].

Commercial applications of ferrofluids date back to the foundation of Ferrofluidics Corporation in 1968 [4]. As a magnetic fluid can be magnetically placed in the gap space between two objects without blocking their relative movement, ferrofluids have been used for sealing in rotary shafts and other mechanical components [4,7–9]. Technological uses include lubrication [10], sensor devices [11–13], thermodiffusion [6], among many others that involve magnetically detecting, positioning or moving [3]. Biomedical applications include magnetic hyperthermia [14,15], drug targeting [16,17], and others.

Loss of colloidal stability could undermine technological and biomedical applications of ferrofluids. Therefore, route synthesis are specially designed to enhance the nanoparticles' mutual repulsion. The oil-based ferrofluid is the most commonly used for technological applications. The nanoparticles of this colloid are surfacted by amphiphilic molecules, such that the polar heads remain attached to the nanoparticle surfaces while the apolar tails stretch toward the solvent, as in a reverse micelle. On the other hand, if the application involves dispersing the magnetic particles in a polar solvent, the stabilization might be provided by charge generation through chemical reactions on the nanoparticle surfaces [18,19]. However, the nanoparticle's charge is usually dependent on pH, being close to zero in neutral solution, leading to agglomeration [20]. This effect might cause a sol-gel transition in the ferrofluid, which hinders its usage in biological applications. Furthermore, a wide range of complications to the host could be caused by particle agglomeration or the presence of excessively big nanoparticles [21,22]. A solution for this problem is to treat the nanoparticles with an ionic surfactant [18]. Ionizable groups at the free extremities of the surfactant molecules are more prone to ionization than ionizable groups on nanoparticle surfaces. Thus, the so-called ionic surfacted nanoparticles are charged at neutral pH and might be dispersed in electrolytic water as a physiological medium.

Computer calculations have long been used to study the particle structure on magnetic fluids, with the employment of different methods such as Monte Carlo simulations [23,24], stochastic dynamics [25–27] and entropy calculations [26,28]. Early bidimensional simulations showed the formation of long chains [23,29,30] by considering pairs of

smaller clusters or isolated particles. That procedure is understandable since most particle interaction models do not include small-range attractive forces or nanoparticle merging. Other approaches include Lennard-Jones potential [26,31,32], rigid rod steric repulsion [33,34] and a hard sphere model with impenetrable surfactant layers [35].

In this work, we propose an interaction model with a more detailed approach to small particle separations, including Born-Mayer repulsion and cohesion energy, and perform Monte Carlo simulations to investigate its descriptive power. For the sake of comparison, we also perform simulations using a previous model consisting of the traditional DLVO interactions with the addition of magnetic dipolar and steric interactions [24,36–38]. Our reference system is a magnetic colloid composed of magnetite nanoparticles coated with tartrate and dispersed in water, whose samples were studied by Bakuzis and co-workers [24] with the aim of investigating the influence of the aging process on particle agglomeration. In order to simulate these samples and some theoretical variations of them, we carried out modifications on the XDLVO model used by the authors, towards a more detailed description of the interaction between particles with small intersurface separations. We implemented a recent improvement of Schnitzer and Morozov [39] to the electrical double layer (EDL) interaction that extends the domain of validity of Derjaguin approximation. We also proposed a new approach to the van der Waals interaction at intersurficial distances of the order of the molecular structure of the nanoparticles, including cohesion energy and Born-Mayer repulsion. Our results show that such improvements enhance the physical description of nanoparticle agglomeration in ferrofluids.

2. Particle interaction models

2.1. Model 1: DLVO + ster + mag

The stability of colloids is traditionally modeled by means of the DLVO theory,² which describes the interaction between a pair of colloidal particles as the balance between a van der Waals attraction and an electrical double layer repulsion. The name XDLVO applies to any extension of the DLVO, having little discriminating power. Thus, we shall call the XDLVO that adds steric and magnetic interparticle interactions to the DLVO model as “DLVO + ster + mag” or simply “model 1”.

The van der Waals interaction energy between two spherical particles of radii R_i and R_j is written as [40]

$$U_{vdw(ij)} = -\frac{A}{6} \left[\frac{2R_i R_j}{r_{ij}^2 - (R_i + R_j)^2} + \frac{2R_i R_j}{r_{ij}^2 - (R_i - R_j)^2} + \ln \left(\frac{r_{ij}^2 - (R_i + R_j)^2}{r_{ij}^2 - (R_i - R_j)^2} \right) \right], \quad (1)$$

where A is the Hamaker constant, and r_{ij} is the distance between the nanoparticles' centers.

$$U_{edl(ij)} = \frac{64\pi c(k_B T)^2}{e^2} \tanh \left(\frac{e\psi_i}{4k_B T} \right) \tanh \left(\frac{e\psi_j}{4k_B T} \right) \left[\frac{R_i R_j}{R_i + R_j} \right]^2 \times \exp \left(-\frac{s_\sigma}{\lambda_D} \right), \quad (2)$$

nanoparticles as bonded to each other when their surface distance were less than a certain distance, such that clusters would never break into

¹ Ferromagnetism is used here in the broader sense that includes ferrimagnetism.

The EDL repulsion, in turn, is given by [41,42]

where e is the electric permittivity of the solvent, k_B is the Boltzmann

² DLVO: Derjaguin-Landau-Verwey-Overbeek.

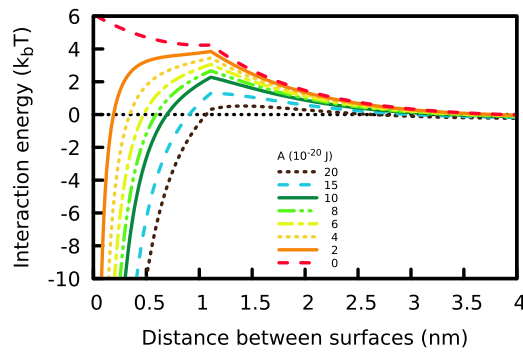


Fig. 1. Interaction energy curves for magnetic nanoparticles of diameters $D_i = D_j = 7.17 \text{ nm}$ ($R_i = R_j = 3.585 \text{ nm}$), with magnetic dipoles aligned head-to-tail, as a function of their surface-surface separation, using the parameters listed in Appendix A wherever applicable. The total energy diverges towards minus infinity as the surface distances tends to zero, requiring the definition of a short cutoff distance.

constant, T is the absolute temperature, e is the elementary charge, ψ_i and ψ_j are the electric potential values on the surface of the i -th and j -th spheres, s_σ is the distance between the charged surfaces, and λ_D is the Debye length, given by

$$\lambda_D = \left(\frac{e k_B T}{\rho_{ion} z_{ion} e^2} \right)^{1/2}, \quad (3)$$

where ρ_{ion} is the ion concentration in the solvent, and z_{ion} is the valence of the ions in the solution (we have used $z_{ion} = 1$ in this work).

The distance s_σ might coincide with the surfaces of the particles themselves, but ionic-surfaced nanoparticles frequently have their charges located at the outer extremities of the surfactant molecules. In such a situation, the surface charge density σ is over a sphere of radius $R + \delta$. For intersurface distances shorter than 2δ , the surfactant layers are in physical contact, such that the electrical double layer force is not well defined anymore and a new steric repulsion arises, due to the overlap between neighbor surfactant layers. This steric repulsion is written as ([33,34] *apud* [2])

$$U_{ste(ij)} = \frac{\pi \xi k_B T}{2} 4R_{ij}^2 \left[2 - \frac{(r_{ij} - 2R_{ij})}{\delta} - \frac{r_{ij}}{\delta} \ln \left(\frac{2(R_{ij} + \delta)}{r_{ij}} \right) \right], \quad (4)$$

where ξ is the grafting parameter (surface density of adsorbed molecules), R_{ij} is the arithmetic mean of the two nanoparticle radii (R_i and R_j), and δ is the length of the surfactant layers.

The nanoparticles of magnetic colloids (ferrofluids) also interact through the magnetic dipolar interaction, written as [2]

$$U_{mag(ij)} = \frac{\mu}{4\pi} \left[\frac{\overrightarrow{m}_i \cdot \overrightarrow{m}_j - 3(\overrightarrow{m}_i \cdot \hat{r}_{ij})(\overrightarrow{m}_j \cdot \hat{r}_{ij})}{r_{ij}^3} \right]. \quad (5)$$

Here, μ is the magnetic permeability of the solvent, \overrightarrow{m}_i and \overrightarrow{m}_j are the nanoparticles' magnetic moments, and \vec{r}_{ij} is the distance vector between them. For each nanoparticle, magnetic moment is given by $\overrightarrow{m}_i = MV_{mag(i)} \hat{u}_i$ [2] where \hat{u}_i is the unit vector along the nanoparticle magnetic moment direction, M is the magnetization of magnetite, and $V_{mag(i)}$ is the "magnetic volume" of the nanoparticle, given by

$$V_{mag(i)} = \frac{4\pi}{3} (R_i - \delta_s)^3, \quad (6)$$

where R_i is the radius of nanoparticle i and δ_s is the length of its nonmagnetic shell.

In this paper, we shall refer to **model 1** (DLVO + ster + mag) as the inclusion of the terms given by Eqs. (1), (2), (4) and (5) in the total interaction energy between the nanoparticles of the magnetic colloid.

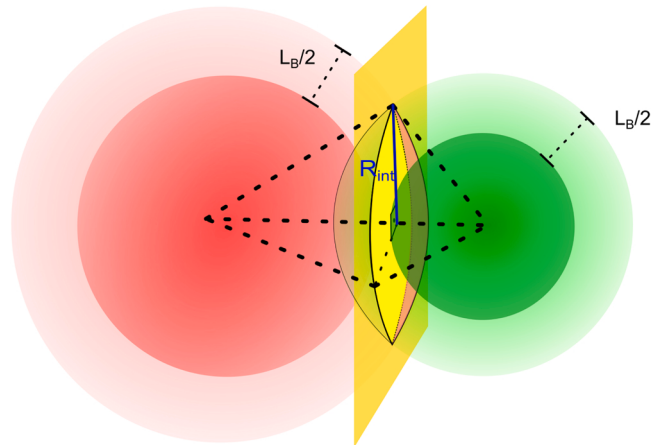


Fig. 2. Illustration of the area between two spherical nanoparticles through which atomic bonds can be formed. The yellow disk between the spheres has area $A_{int} = \pi R_{int}^2$ and corresponds to intersurface distance shorter than maghemite atomic bond distance (L_B).

This is practically the same model as used by Bakuzis and co-workers [24], with the difference that we include the core-shell effect on particle magnetization by means of the nonmagnetic shell length δ_s (also called *excluded diameter*) in Eq. (5), causing overall lower interparticle magnetic interaction. Fig. 1 shows the energy curves of model 1 for a pair of nanoparticles using the parameters listed in Appendix A. The colloidal nanoparticles of this system have their charge located at the outer extremity of the surfactant layer. As the nanoparticles come close enough, so that the surfactant layers can overlap, the EDL energy remains constant and the steric repulsion comes into place. Keeping the EDL interaction energy constant in this range is the most prudent choice in the absence of a more detailed model, because setting it equal to zero could give rise to an artificial potential well.

In addition to the inter-particle interaction so far described, each particle also interacts with a magnetic field of external origin, as described by the Zeeman energy

$$U_{ze(i)} = -\overrightarrow{m}_i \cdot \overrightarrow{B}, \quad (7)$$

where \overrightarrow{m}_i is the magnetic dipole moment of the particle i and \overrightarrow{B} is the magnetic field vector.

In summary, the total energy of the system, as described by model 1, reads

$$U_{M1} = \sum_{i=1}^N U_{ze(i)} + \sum_{i=1}^N \sum_{j=i+1}^N [U_{vdw(ij)} + U_{edl(ij)} + U_{ste(ij)} + U_{mag(ij)}]. \quad (8)$$

2.2. Model 2: DLVO + ster + mag + BM + SM

With the purpose of describing the small-distance regime more realistically, we propose another model, called model 2, which consists of modifications in the van der Waals and EDL energy terms of model 1, while keeping the rest unaltered. For pairs of particles with small separations, model 2 keeps van der Waals energy term constant and add terms related to cohesion energy and Born-Mayer repulsion. Concerning the EDL repulsion term, its accuracy was improved by using an alternative formula deduced by making use of a generalization of the Derjaguin approximation by Schnitzer and Morozov [39]. In reference to the Born-Mayer repulsion and the Schnitzer-Morozov corrections, we also call model 2 as "DLVO + ster + mag + BM + SM". We also include a cohesion energy term that we shall ignore in this label for the sake of conciseness.

Eq. (1) was obtained by integrating a sixth-power law interaction ($u(r) \propto r^{-6}$) over the volume of the two spheres [40], disregarding the

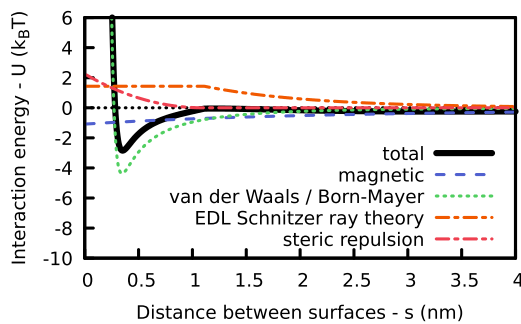


Fig. 3. Interaction energy curves for colloidal magnetic nanoparticles of diameters $D_i = D_j = 7.17 \text{ nm}$ ($R_i = R_j = 3.585 \text{ nm}$), as a function of their surface-surface separation, using the parameters listed in Appendix A wherever applicable. Here, the total energy increases as the surface distances tends to zero, which is not an obstacle to Monte Carlo simulations, since high-energy configurations are avoided by construction.

discrete nature of their atomic structure, meaning that it is not valid for surface-surface distances of the order of atomic bonds. Thus, for surface-surface distances shorter than a certain critical distance, we fixed the van der Waals interaction energy and added a cohesion energy given by

$$U_{coh} = A_{int} W_{coh}, \quad (9)$$

where A_{int} is the area between the spheres as their surfaces are close enough to form atomic bonds and W_{coh} is the work of cohesion. The reference system of our simulations is composed of magnetite nanoparticles, but their shell become maghemite by oxidation [24]. The area A_{int} is calculated as the area of intersection between spheres i and j with their radii increased by half of a maghemite atomic bond distance ($L_B/2$), so that

$$A_{int} = \pi R_{int}^2 \quad (10)$$

where R_{int} is calculated as

$$R_{int} = \frac{1}{2r_{ij}} [(-r_{ij} + R_i - R_j)(-r_{ij} - R_i + R_j)] \times (-r_{ij} + R_i + R_j + L_B)(r_{ij} + R_i + R_j + L_B). \quad (11)$$

and illustrated in Fig. 2.

Nevertheless, we also expect a strong repulsion as the electron from neighbor shells overlap. Given the surfaces' shape, we consider here that such repulsion will occur for only a pair of atoms at a time. Thus, the repulsion is modeled by means of a Born-Mayer potential [43]:

$$U_{bm} = A_{bm} \exp(-s_{ij}/L_{bm}), \quad (12)$$

where the values of A_{bm} and L_{bm} were taken from a derivation for a Fe^{2+}

+ O^{2-} bond [43]. The parameters for $Fe-O$ are intermediate between those for $Fe-Fe$ and $O-O$, such that they reasonably describe an average repulsion between the closest atoms of the nanoparticle pairs.

Therefore, model 2 replaces the van der Waals term of each ij pair in Eq. (1) with the following energy term

$$U_{vdw-bm(ij)} = \begin{cases} U_{vdw(ij)}(L_B) & \text{if } s_{ij} > L_B, \\ U_{vdw(ij)}(L_B) + U_{coh(ij)} + U_{bm(ij)} & \text{otherwise} \end{cases} \quad (13)$$

where $U_{vdw(ij)}(L_B)$ is the value of $U_{vdw(ij)}$ for $r_{ij} = L_B$.

Eq. (2) is known to be unsuitable for small distances. In order to circumvent this limitation, we have derived an alternative expression for the EDL interaction by using Schnitzer and Morozov's generalization [39], extending the validity of the expression to all separations. By integrating the force, we get the following interaction energy expression:

$$U_{edl-sm(ij)} = 128\pi\lambda_D(k_B T)^2 \rho_{ion} \tanh\left(\frac{e\psi_i}{4k_B T}\right) \tanh\left(\frac{e\psi_j}{4k_B T}\right) Ei\left(-\frac{r_{ij} - 2\delta}{\lambda_D}\right), \times e^{(R_i + R_j)/\lambda_D} \quad (14)$$

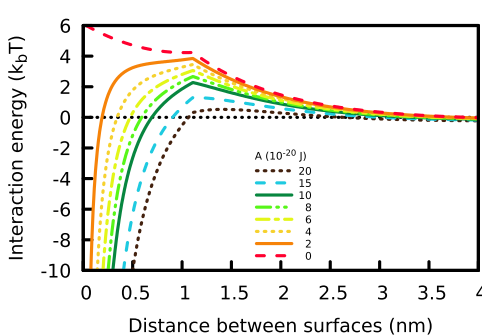
where ρ_{ion} is the ion concentration in the solvent, ψ_i and ψ_j are the electric potential values on the surface of the spheres, Ei is the exponential integral function, and λ_D is the Debye length.

In comparison to the model whose energy curves are shown in Fig. 1 (model 1, DLVO + ster + mag), the modified model (model 2, DLVO + ster + mag + BM + SM) has energy curves that seem to deliver a more adequate physical description of this system. As seen in Fig. 3, the divergence in small distances is now absent and the curves have a clear potential well.

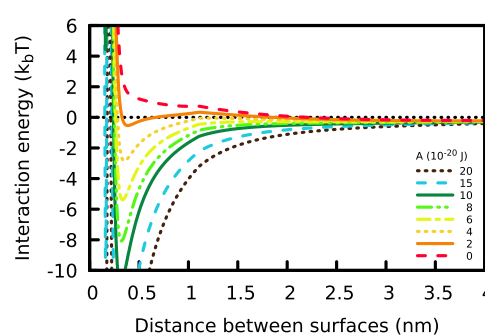
Fig. 4 shows the interaction energy between a pair of magnetic colloidal nanoparticles of diameters $D_i = D_j = 7.17 \text{ nm}$, as a function of their surface-surface separation, for variable Hamaker constant A (from $1 \times 10^{-20} \text{ J}$ to $20 \times 10^{-20} \text{ J}$). This range of possible values for the effective Hamaker constant was estimated by Bakuzis and co-workers, considering effects of particle surface oxidation and the variable amount of surfactant molecules between the two nanoparticles [24]. The simulations of this work have $A = 4 \times 10^{-20} \text{ J}$, as used previously by Castro et al. [38]. Fig. 4a displays the curves for model 1, while Fig. 4b shows the curves for model 2 that gets rid of the minus infinity divergence.

In summary, the total energy of the system, as described by model 2 (DLVO+ster+mag+BM+SM), becomes

$$U_{(M2)} = \sum_{i=1}^N U_{zee(i)} + \sum_{i=1}^N \sum_{j=i+1}^N [U_{vdw-bm(ij)} + U_{edl-sm(ij)} + U_{ste(ij)} + U_{mag(ij)}]. \quad (15)$$



(a) model 1 (DLVO+ster+mag)



(b) model 2 (DLVO+ster+mag+BM+SM)

Fig. 4. Curves of interparticle total interaction energy for colloidal magnetic nanoparticles of diameters $D_i = D_j = 7.17 \text{ nm}$ ($R_i = R_j = 3.585 \text{ nm}$), as functions of their surface-surface separation, for model 1 (a) and model 2 (b). The interaction parameters are as shown in Appendix A, except for the Hamaker constant, which varies from 0 to $20 \times 10^{-20} \text{ J}$, as the legend shows. The lower EDL repulsion and absence of divergence to minus infinity makes model 2 more suitable for Monte Carlo simulations.

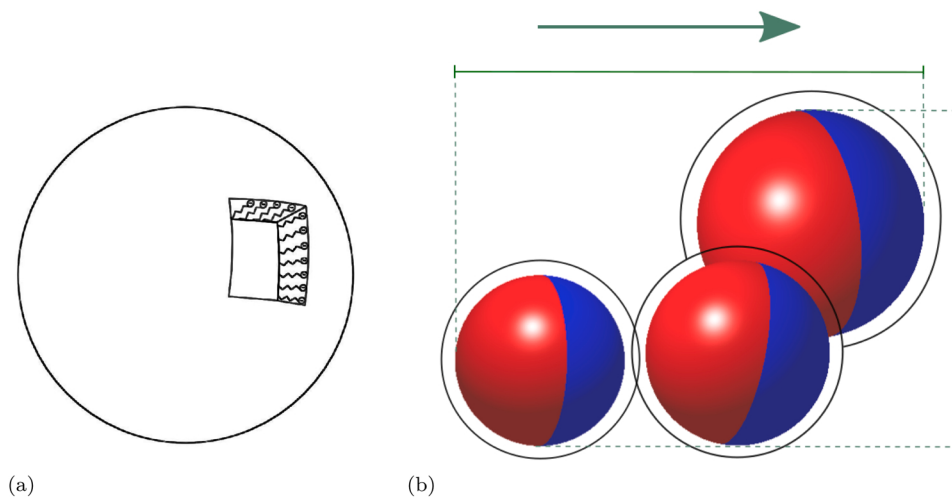


Fig. 5. Illustration of an ionic-surfacted nanoparticle and an agglomerate. (a) Ionic-surfacted nanoparticle. The surfactant molecules have apolar tails attached to the nanoparticle surface and polar heads that tend to disperse into the surrounding medium. As a result, the molecules stretch themselves radially from the particle toward the solvent. The charged surface is not on the nanoparticle itself, but at the outer extremities of the surfactant molecules. (b) Agglomerate formed by three nanoparticles. The blue and red hemispheres represent the magnetic poles of the particles. The black circles indicate the reach of the maximum extent of the surfactant molecules around each particle. In green, the figure represents the applied magnetic field (\vec{B}) and agglomerate lengths parallel and perpendicular to \vec{B} . Two particles belong to the same agglomerate when there is intersection between their surfactant layers.

2.3. Limitations of the models

Due to the size of the simulated system, we opted for mesoscopic models that do not explicitly describe some molecular scale phenomena. The EDL repulsion expressions (Eqs. (2) and (14)) consider an homogeneous ion distribution. At small distances between charged surfaces, microscopic effects such as the finite size of hydrated ions, multiple counterion-coion layers and counterion condensation might become important [44–47]. However, the colloidal particles of our reference system are charged at the outer extremities of the surfactant layers, such that, when the surfactant layers of two nanoparticles overlap, the repulsion between the charges could cause an effective attraction between the nanoparticles, instead of a repulsion. As the surfactant charges may cause repulsion or attraction between the nanoparticles, depending on their position relative to both surfaces, an accurate description would require simulations on the atomic level, therefore we choose to keep EDL repulsion fixed for distances for which surfactant overlap is possible.

The models used in this work consider that the surfacted amphiphilic molecules are stretched towards the solvent, as Fig. 5a shows. The surfactant molecules are relatively short and perform a stochastic pendular motion. In this condition, there is no necessity to use a more complex description of the surfactant or quantities such as Flory characteristic ratio, usually used to describe the gyration ratio of entangled polymeric surfactant [44,48]. In spite of the particularities of the system simulated here, the modifications proposed in model 2 represent a general refinement of the DLVO theory to which microscopic effects may be included further.

The nanoparticles themselves also present surface irregularities, possibly modifying short-range interactions. Theoretical developments show that the intensity of such effects ultimately depends on the root-mean-squared (RMS) roughness [49–51], which varies largely depending on the nanoparticle's composition and the synthesis route. For instance, previous works report ferrofluid's intrinsic low RMS roughness around 2 Å–4 Å [52]. On the other hand, film conformations can dramatically increase the systems' RMS roughness, leading to values over 50 nm–100 nm [53,54], potentially affecting short-range interactions. Furthermore, throughout this work, we will assume the magnetic nanoparticles to be hard spheres of infinite stiffness. By doing so, we also neglect elastoplastic effects on surface asperities. We believe that is not an issue since current experimental evidence does not indicate any expressive macroscopic elastoplastic effects on ferrofluids [55], oppositely from other nanoparticle-based systems [56,57].

3. Simulation

The simulation of the ferrofluid was performed by means of a Monte

Carlo method, using the interaction energy curves presented in Section 2 and the parameters listed in Appendix A. Systems at different particle concentrations were modeled as spheres inside a cubic box with periodic boundary conditions. For each simulation, the number of spheres (N) and the box side (L) were chosen in such a manner that the volume fraction (ϕ) coincides with experimental values when calculated through the relation

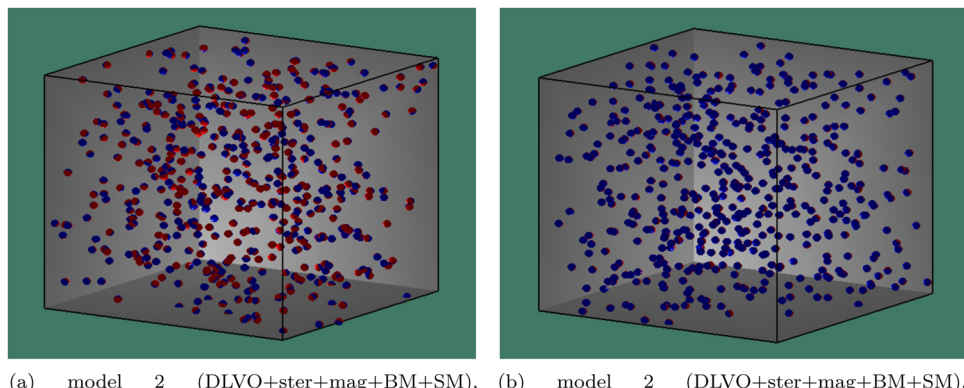
$$\phi = \frac{\sum_i V_i}{L^3} \quad (16)$$

where the summation is taken over the volumes of all spheres (V_i). In each simulation, the value of N was initially set to 500, while the value of L was calculated in such a way that the volume fraction represents the experimental data. Then, if necessary, the program increased the value of N to ensure a minimum of 150 nm for L , which was then finely adjusted to keep the same ϕ . Our program also simulates ensembles of polydisperse spheres by distributing their diameters stochastically according to a log-normal probability density function

$$p(D) = \frac{1}{\sqrt{2\pi}\sigma D} \exp\left(-\frac{-\ln^2(D/D_0)}{2\sigma^2}\right). \quad (17)$$

Once the nanoparticle diameters are fixed, the program generates a sample of particle configurations (sets of positions and orientations) by means of a Metropolis-Hastings algorithm [58,59] (also called simply Metropolis algorithm), considering that (1) the system is in thermal equilibrium at room temperature $T = 300$ K, (2) the nanoparticles interact with an applied magnetic field \vec{B} and (3) the nanoparticles interact with each other through the interactions shown in Section 2. The total interaction energy of a certain configuration is given by Eq. (8) in simulations using model 1 or Eq. (15) in simulations using model 2. As the Metropolis algorithm does not function properly with the energy divergence of $U_{vdw(ij)}$ (Eq. (15)), a minimum intersurface distance (s_{min}) was set to 0.01 nm. The main properties of the interaction energy curves are still covered by the model with this minimum.

The Metropolis algorithm operates in Monte Carlo (MC) steps, starting from a random configuration of the system. Each MC step includes a random modification of the system variables and a test that determine if the modification is accepted. The random modification consists of small changes in all particle positions and orientations, which causes a small variation of the configuration energy U . In each MC step, the modification is accepted if the energy variation ΔU is negative. Whenever ΔU is positive, the probability of accepting the modification is weighted by $f = e^{-\frac{\Delta U}{k_B T}}$ in that MC step. This probability is executed by comparing f with random number a in the $[0,1]$ interval; the modification is accepted if f is greater than a . If the modification is rejected, the



(a) model 2 (DLVO+ster+mag+BM+SM), monodisperse, zero field
 (b) model 2 (DLVO+ster+mag+BM+SM), monodisperse, field $B = 1$ T

Fig. 6. Snapshots of Monte Carlo simulations of the reference system without diameter polydispersity, at zero field (a) and at $B = 1$ T, using model 2 (DLVO + ster + mag + BM + SM). The direction of field is at the back-to-front direction. The interaction parameters are as shown in Appendix A. The magnetic poles are represented as blue and red hemispheres. The particles look almost monochromatic in the figure on the right due to the alignment along the magnetic field.

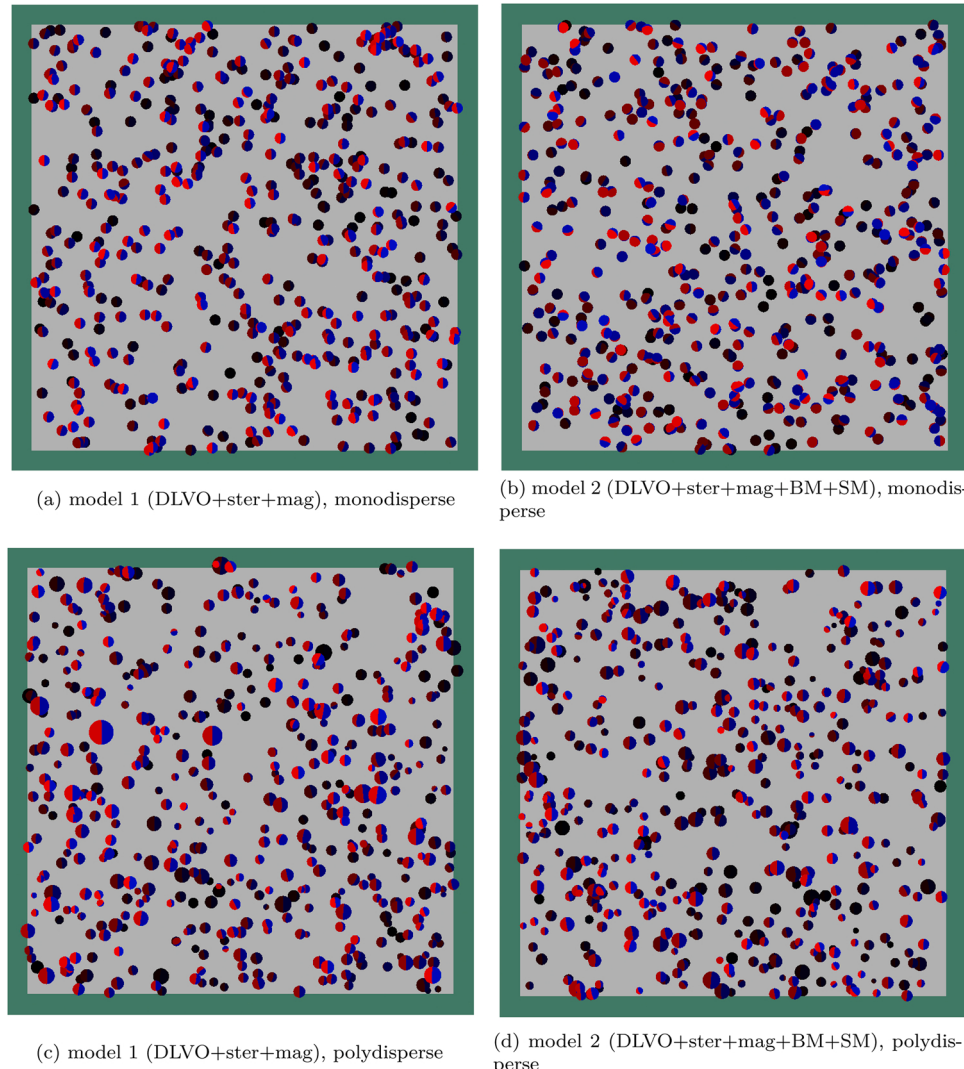


Fig. 7. Snapshots of Monte Carlo simulations of ferrofluid samples with monodisperse (a, b) and polydisperse (c, d) diameter nanoparticles, using the model 1 (a, c) and model 2 (b, d). The interaction parameters are as shown in Appendix A. The magnetic field ($B = 1$ T) is applied in the left-to-right direction.

unmodified configuration is used in the next MC step. This procedure guarantees that the generated configurations follow a Boltzmann distribution [58,59].

The program dynamically adjust the maximum variation in position and orientation coordinates considering a target acceptance rate (α) of 0.5, which means that approximately 50% of the modifications are

Table 1

Average first neighbor surface distance ($\langle s_1 \rangle$) for different models and systems, with $\phi = 0.0047$ and $B = 0$ and $B = 1$ T. For the zero field condition, there is a systematic decrease from non-magnetic to magnetic systems when using model 2 (DLVO + ster + mag + BM + SM), which is not observed in model 1 (DLVO + ster + mag). For $B = 1$ T, both models give similar results.

$B = 0$		Average first neighbor surface distance (nm)			
		Monodisperse		Polydisperse	
		Non-magn.	Magnetic	Non-magn.	Magnetic
model 1	11.7	11.8	13.3	13.4	
model 2	12.1	11.7	14.4	13.5	
$B = 1$ T		Average first neighbor surface distance (nm)			
		Monodisperse		Polydisperse	
		Non-magn.	Magnetic	Non-magn.	Magnetic
model 1	–	12.5	–	13.9	
model 2	–	12.3	–	13.7	

accepted throughout the simulation. After the total interaction energy of the system stabilizes, the program starts a sampling process to calculate the average values of quantities of interest over a number of MC steps. The beginning and end of the sampling process are determined by the minimum energy ever reached by the system. For every 50,000 MC steps, the variation of the minimum energy ever reached in the simulation (ΔU_{\min}) is computed. The sampling process initiates when the relative variation $\Delta U_{\min}/U_{\min}$ is lower than 0.05 and finishes when it is lower than 0.005, guaranteed a minimum of 50,000 sampling MC steps. The averaging of the physical quantities of interest is performed over the sampled configurations, whose acceptance is determined by the total potential interaction energy, through the Boltzmann factors $e^{-\frac{U}{kT}}$. Thus, one takes the averages as the expected values of the physical quantities investigated, which may be analyzed and compared to other results from experiment and theory. Alternative descriptions of the Metropolis algorithm as applied to polydisperse magnetic nanoparticles are found in previous papers [24,36,38].

4. Results

It is useful to visualize some snapshots of the simulations, such as the ones shown in Fig. 6 for a monodisperse variation of the reference system at zero field (Fig. 6a) and $B = 1$ T (Fig. 6b). The nanoparticles are represented by spheres, whose blue and red indicate north and south magnetic poles. At the zero field regime, one can observe that the particles' orientation shows no preferred direction, as expected. Regardless, due to interparticle interactions, agglomeration occurs even in such conditions. At the strong magnetic field regime, the particles' magnetic moment dipoles align with the field, an effect visualized in Fig. 6b as the spheres' blue sides points toward the front face.

By looking at Fig. 6, one may have the impression of an overestimated agglomeration. This is due to the difficulty in account the distance between neighbor nanoparticles under a three-dimensional perspective. In fact, some particle pairs are separated by a distance that is longer than revealed by the figure. In order to overcome this difficulty, we changed the point of view such that the magnetic field (B) is directed from the left to the right and the distance from the observer is indicated by the darkness of each particle, as seen in Fig. 7. The figure shows snapshots of Monte Carlo simulations of different variations of the reference system, subject to a magnetic field of 1.0 T from an external source. One can notice that the monodisperse nanoparticles form more packed structures, as confirmed by the average surface distance between first neighbors ($\langle s_1 \rangle$) shown in Table 1, which also includes the $\langle s_1 \rangle$ results for non-magnetic systems. This might have been caused by the higher steric and EDL repulsions between larger nanoparticles, which are absent in the monodisperse system. It is true that nanoparticles with

Table 2

Agglomerate dimensions and relative elongation for samples at $B = 1$ T.

$\delta_s = 0.8$ nm	Dispersity	$D_{\parallel}^{\text{agg}}$ (nm)	D_{\perp}^{agg} (nm)	$D_{\parallel}^{\text{agg}}/D_{\perp}^{\text{agg}}$
model 1	mono	11.75	11.11	1.058
	poly	10.87	10.42	1.044
model 2	mono	11.55	11.53	1.002
	poly	14.32	12.87	1.113

$\delta_s = 0$	Dispersity	$D_{\parallel}^{\text{agg}}$ (nm)	D_{\perp}^{agg} (nm)	$D_{\parallel}^{\text{agg}}/D_{\perp}^{\text{agg}}$
model 1	mono	11.38	11.51	0.989
	poly	12.60	12.25	1.029
model 2	mono	12.61	11.01	1.146
	poly	14.99	11.78	1.272

diameters smaller than the modal value are also absent in the monodisperse samples, but the log-normal distribution of the polydisperse samples is right-skewed (Eq. (17)). Another potential cause for such effect is the tendency for higher agglomeration among similar particles, a theoretical result obtained for particles that interact via finite attractive interaction energy [44].

One can also notice in Table 1 that, when $B = 0$, the findings for the DLVO+ster+mag model are indistinguishable for magnetic and non-magnetic colloids, while there is a systematic distance decrease from non-magnetic to magnetic when using the DLVO + ster + mag + BM + SM model. For the high field of 1 T, the interaction of the particles with the applied field becomes more relevant than the interparticle interactions. Consequently, both models deliver similar results, suggesting that, for such field regime, the contact-based interactions are less significant for the colloidal stability.

In spite of the similar results of the models for $\langle s_1 \rangle$, model 2 reveals important differences of agglomeration structure between monodisperse and polydisperse systems, as shown in Table 2. Two nanoparticles were considered as belonging to the same agglomerate when there was an overlap between their surfactant layers, which characterizes physical contact. The quantities $D_{\parallel}^{\text{agg}}$ are averages of the agglomerate lengths depicted in Fig. 5b, $D_{\parallel}^{\text{agg}}$ being this extension along the applied field \vec{B} , while D_{\perp}^{agg} is measured in the perpendicular direction.³ The results for model 1 (DLVO + ster + mag) show similar values for monodisperse and polydisperse systems. In contrast, model 2 resulted in a small difference between the two types of system. Average agglomerate dimensions are larger in the polydisperse system and the clusters are also more elongated in the field direction. The agglomerates are slightly larger for nanoparticles without the non-magnetic shell (vide Fig. 9), although the pattern of variation is similar. Once more, model 1 resulted in similar values for the elongation, while there is a more noticeable difference for model 2. These results are coherent with the agglomerate dimensions estimated by Paula [60], using SAXS data for a colloidal dispersion of manganese ferrite nanoparticles with similar diameter distribution at approximately 0.5 T. Paula's results correspond to agglomerate elongation between 1.4 and 1.8, which can be considered as relatively similar to our results when the differences between the systems are taken into account.

It is important to note that Figs. 8 and 9 show only one among thousands of sampled configurations in each simulation. The nanoparticles are in frequent movement during the simulation, such that clusters form and dissipate. Most of the agglomerates displayed are dimers, although they can unite and form larger agglomerates in some configurations. Due to the low particle concentration of the system, dimers are much more probable to occur than longer clusters. One can also note that the particle alignment is not perfect. This is not surprising if one look at the energy curves of Fig. 3 for two particles with the modal

³ D_{\perp}^{agg} was averaged over particles and directions, since there are infinite possible directions perpendicular to \vec{B} .

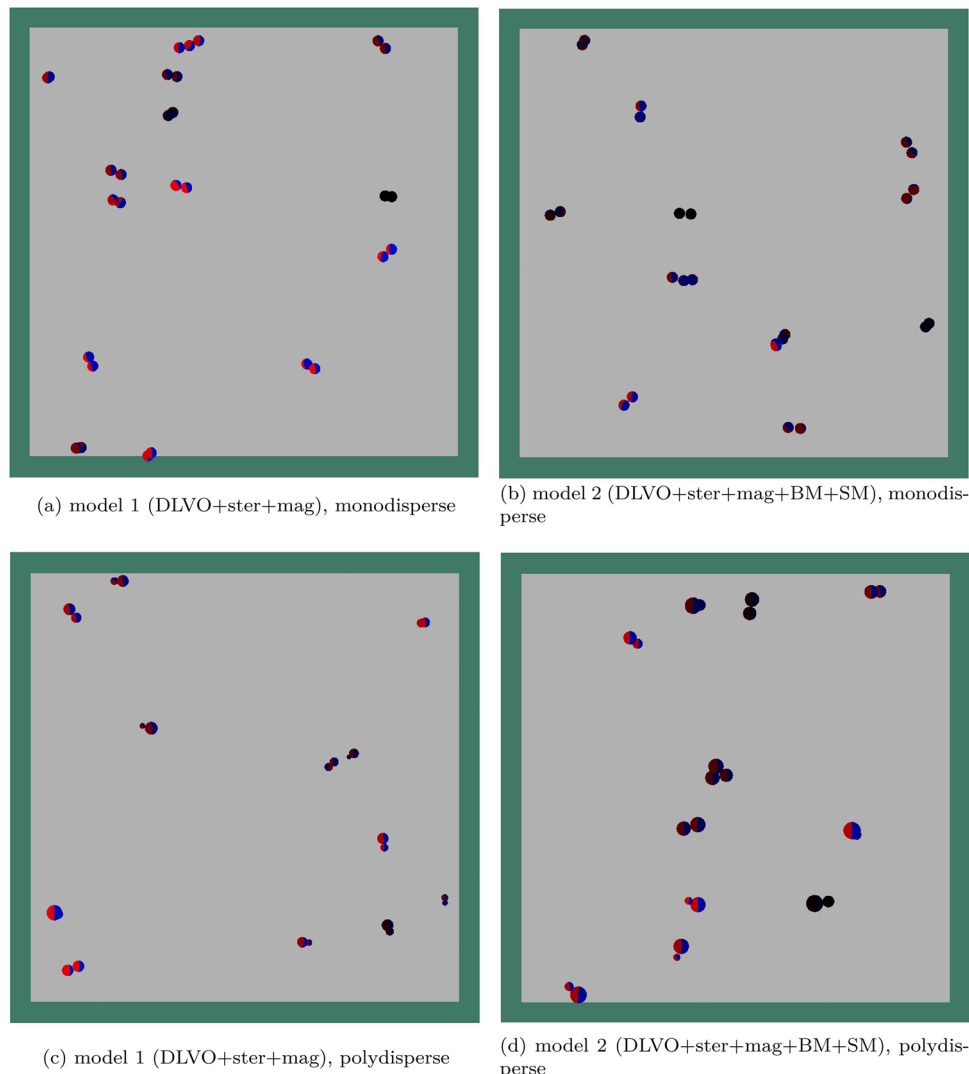


Fig. 8. Agglomerates present in the configurations shown in Fig. 7: monodisperse (a, b) and polydisperse (c, d) diameter nanoparticles, using model 1 (a, c) and model 2 (b, d). The interaction parameters are as shown in Appendix A. A magnetic field ($B = 1$ T) is applied in the left-to-right direction.

diameter in the head-to-tail configuration. The magnetic interaction is close to $1k_B T$ at its maximum (zero surface distance), not sufficient to maintain the pair united. One can also conclude that thermal agitation in such conditions will permit large angles between any vector pair among \vec{m}_i , \vec{m}_j and \vec{r}_{ij} of Eq. (5).

We noted in the simulations with model 1 that the particles practically stop changing their positions when they bond to each other. Once a particle agglomerates, its movement is mainly rotational. Such behavior is absent in model 2 simulations, for which there is no notable difference of mobility between aggregated and isolated particles. This difference might be explained through the curves of Fig. 4. As two nanoparticles approach, their interaction energy becomes extremely negative, in such a way that the program rejects most modifications that would change their relative position, because even small displacements cause great energy variations. Although this could be avoided by means of a carefully chosen short-range cutoff distance (as done in the reference study [24]), the optimal value would depend on characteristics of the given colloidal specimen, greatly undermining the model's applicability to different systems. In face of this crippling limitation, we turn to model 2 as a reliable solution that does not suffer from such tight restrictions.

In order to investigate the agglomeration process, we display the pair correlation function for the monodisperse and polydisperse systems with $\phi = 0.47\%$ in Fig. 10. In the monodisperse system, the first peak is more

pronounced and better defined, being more regular around the distance of 10 nm for model 2. As for the polydisperse system, the peak degenerates into many smaller ones, because each nanoparticle pair has a different center-to-center distance when in surface contact. Model 1 produced many peaks for polydisperse nanoparticles at center-to-center distances shorter than the modal diameter $D_0 = 7.17$ nm, a direct effect of the deep potential wells of the interaction energy curve. Such peaks are absent in the results of model 2, as a result of the additional repulsions at small separations.

For non-zero magnetic field, angular correlation functions provide additional information. Fig. 11 shows the radial-angular pair correlation function $g(r, \theta)$ averaged over all agglomerates found in the sampled configurations of the polydisperse at $B = 1$ T, for model 1 (a) and model 2 (b) with $\phi = 0.47\%$. The results evidence higher alignment with the field in the configurations simulated using model 2. From the alternation between yellow and green areas suggests seen in Fig. 11b, one can infer a longer range order for model 2.⁴

⁴ This ordering was even more evident in $g(r, \theta)$ for the monodisperse system.

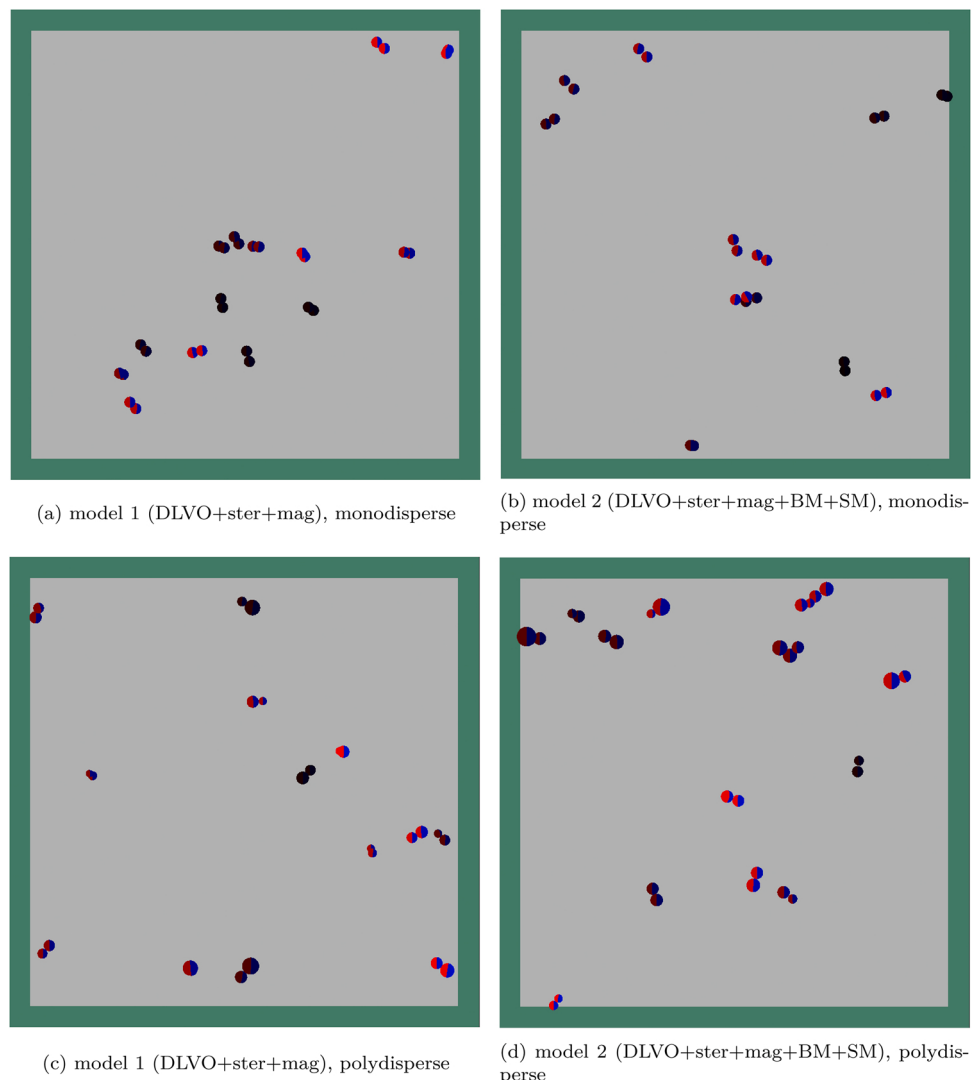


Fig. 9. Agglomerates present in some configurations of nanoparticles without excluded diameter: monodisperse (a, b) and polydisperse (c, d) diameter nanoparticles, using model 1 (a, c) and model 2 (b, d). The interaction parameters are as shown in Appendix A. A magnetic field ($B = 1$ T) is applied in the left-to-right direction.

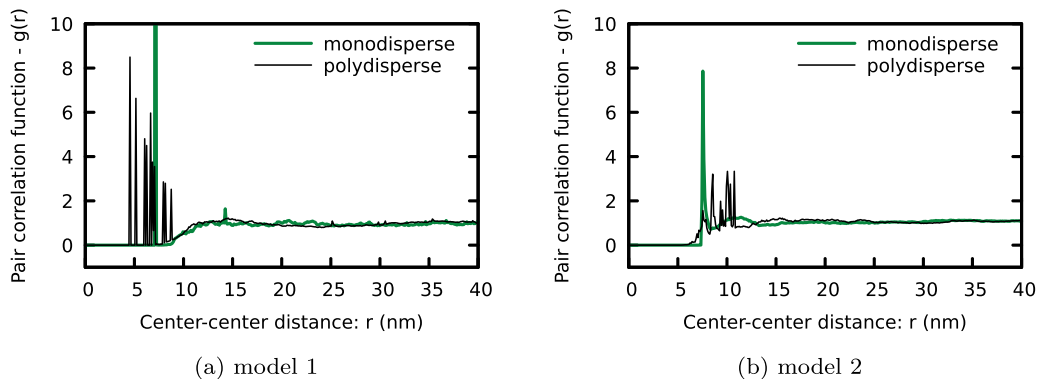


Fig. 10. Pair correlation function for monodisperse and polydisperse systems, for the DLVO + ster + mag model (a) and the DLVO + ster + mag + BM + SM model (b) with $\phi = 0.47\%$. The peak of the traditionally modeled, monodisperse system has a maximum between 40 and 50, while the corresponding peak for model 2 (DLVO + ster + mag + BM + SM) has a maximum value which is closer to those of the polydisperse system.

5. Conclusion

Two models of ferrofluid particle interaction were compared through the results of Monte Carlo simulations. The results of the more

traditional XDLVO model (called here “model 1” or “DLVO + ster + mag model”), which includes steric and magnetic interparticle interactions in the DLVO model, with some adaptations, show no significant difference between magnetic and non-magnetic colloids at zero

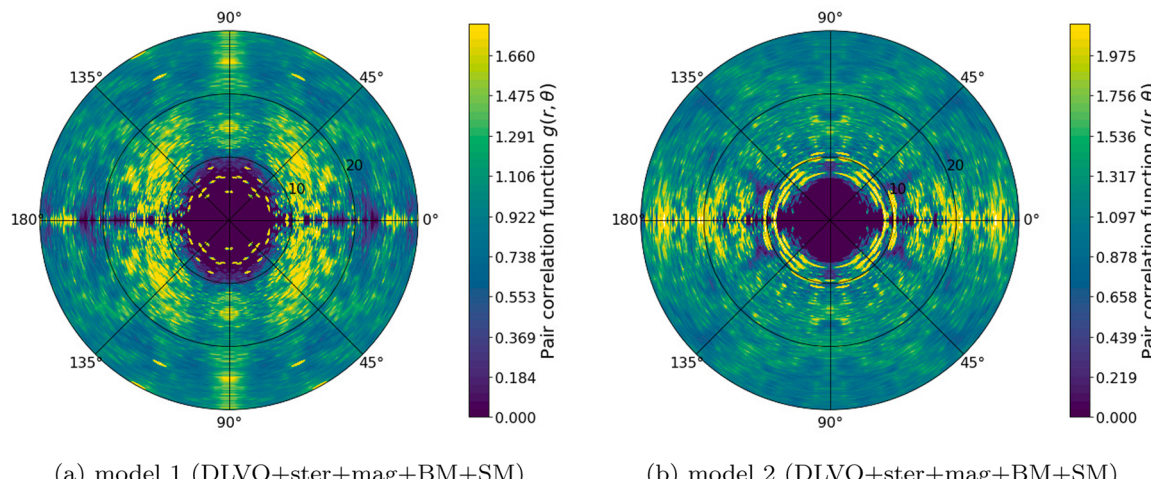


Fig. 11. Pair correlation function $g(r, \theta)$ of the polydisperse systems at $B = 1$ T, for the DLVO + ster + mag model (a) and the DLVO + ster + mag + BM + SM model (b) with $\phi = 0.47\%$. The yellow areas evidence higher alignment with the field in model 2. The alternation between yellow and green areas suggests an order of longer range for model 2.

field. This indicates that the high value of van der Waals and EDL interactions obfuscates the interparticle magnetic interaction, which could give one the impression that they are irrelevant to the agglomeration pattern.

We proposed a new model (“model 2” or “DLVO + ster + mag + BM + SM model”) with the aim of solving that problem with an approach that produces interparticle interactions with similar order of magnitude at small separations. The divergent van der Waals interaction is replaced by means of a more detailed approach that includes cohesion energy and Born-Mayer repulsion. The implementation of a corrected model for the electrical double layer interaction, valid for all interparticle separations, eliminated the pronounced interaction energy maximum around the intersurface separation of 1 nm that appeared in the interaction energy curve of the traditional XDLVO model such that the well-known first and second minima of the DLVO theory could reappear.

The results show that the proposed small separation approach is important to assess the role of the interparticle magnetic interactions effectively. The interaction energy curves and the results are more plausible for the model with the modifications presented in this paper. Simulations with the modified model yielded more realistic results concerning the differences between monodisperse and polydisperse systems, manifested in the results of pair correlation functions and agglomerate structure. Biocompatible magnetic colloids usually have ionic-surfacted nanoparticles in which steric and EDL repulsions are interconnected. In such systems, the limitations of the traditional XDLVO model becomes more evident, and small separation corrections such as the ones shown here are important to perform simulations with reliable results.

Appendix A. System and simulation parameters

The basic parameters used in the simulations to represent the ferrofluid sample as an ensemble of nanoparticles are:

Parameter	Description	Value	Source
N	number of particles	500 (minimum)	
L	box side length	150 nm (minimum)	
T	temperature	300 K	[24]
B	magnetic field	0, 1 T	
D_0	modal diameter	7.17 nm	[24]
σ	diameter dispersion	0.24	[24]

The parameters used in the simulations to describe the interaction energy terms between nanoparticles are:

Variable	Description	Value	Source
μ	magnetic permeability	$1.26 \times 10^{-6} \text{ H m}^{-1}$	
M	nanoparticle magnetization	$4.71 \times 10^{-5} \text{ A m}^{-1}$	[24]
ξ	grafting parameter	$2.0 \times 10^{-17} \text{ m}^{-2}$	[24]
δ	surfactant layer length	0.55 nm	[24]
A	Hamaker constant	$0.40 \times 10^{-21} \text{ J}$	[24]
δ_s	exclude diameter	0.8 nm	
W_{coh} (maghemite)	cohesion energy	1.38 J m ⁻²	[61]
L_B (maghemite Fe-O)	atomic bond distance	0.19 nm	[62,63]
A_{bm}	Born-Mayer parameter A	1207.6 eV	[43]
L_{bm}	Born-Mayer parameter L	0.3084 Å	[43]
λ_D	Debye length	1.1 nm	[24]
ρ_{ion}	ion concentration	0.15 mol l ⁻¹	[24]
ψ	surface electric potential	0.1 V	[24]
s_{min}	minimum intersurface distance	0.01 nm	

The parameters related to the simulation method are:

Variable	Description	Value
$N_{MC[thm]}$	number of thermalization MC steps	50,000
$N_{MC[max]}$	maximum number of MC steps	300,000
$N_{MC[chk]}$	number of MC steps between convergence checks	50,000
ΔU_{ini}	energy variation to initiate sampling process	0.05
ΔU_{fin}	energy variation to finish sampling process	0.005
α	target acceptance rate in Metropolis algorithm	0.5

References

- [1] S.S. Papell, Low viscosity magnetic fluid obtained by the colloidal suspension of magnetic particles, 1965.
- [2] R.E. Rosensweig, Ferrohydrodynamics, Dover, Mineola, New York, 1997.
- [3] R.L. Bailey, Lesser known applications of ferrofluids, *J. Magn. Magn. Mater.* 39 (1983) 178.
- [4] K. Raj, R. Moskowitz, Commercial applications of ferrofluids, *J. Magn. Magn. Mater.* 85 (1) (1990) 233–245, [https://doi.org/10.1016/0304-8853\(90\)90058-X](https://doi.org/10.1016/0304-8853(90)90058-X).
- [5] J. Roger, J.N. Pons, R. Massart, A. Halbreich, J.C. Bacri, Some biomedical applications of ferrofluids, *Eur. Phys. J. - Appl. Phys.* 5 (3) (1999) 321–325, <https://doi.org/10.1051/epjap:1999144>.
- [6] C. Scherer, A.M. Figueiredo Neto, Ferrofluids: properties and applications, *Braz. J. Phys.* 35 (3A) (2005) 718.
- [7] N. Yamazumi, H. Unozawa, Ferrofluid sealing device, 2001. (<http://www.freepatentonline.com/6305694.html>).
- [8] L.S. Barriss, R.A. Comunale, R.P. Fremgen, A.I. Gurary, T.A. Luse, R.W. Milgate, J. D. Pollock, Rotating disk reactor with ferrofluid seal for chemical vapor deposition, US Patent App. 15/382,216, 2017.
- [9] D.G. Mahoney, W. Helgeland, Magnetic fluid seal with precise control of fluid volume at each seal stage, US Patent 9,816,617, 2017.
- [10] D.K. Verma, P. Chandra, P. Sinha, Theoretical studies in ferrofluid lubrication: a review, *Indian J. Eng. Mater. Sci.* 5 (1998) 396.
- [11] K. Raj, J. Greyson, C. Ionescu, Liquid level monitoring system having ferrofluid pressure sensor, 1997.
- [12] K. Raj, Ferrofluid sensor, 2003. (<http://www.freepatentonline.com/EP0857945B1>).
- [13] D. Zhang, Z. Di, Y. Zou, X. Chen, Temperature sensor using ferrofluid thin film, *Microfluid. Nanofluid.* 7 (2009) 141.
- [14] M. Sato, T. Yamashita, M. Ohkura, Y. Osai, A. Sato, T. Takada, H. Matsusaka, I. Ono, Y. Tamura, N. Sato, Y. Sasaki, A. Ito, H. Honda, K. Wakamatsu, S. Ito, K. Jimbow, N-propionyl-cysteaminylphenol-magnetite conjugate (nprcap/m) is a nanoparticle for the targeted growth suppression of melanoma cells, *J. Invest. Dermatol.* 129 (9) (2009) 2233–2241.
- [15] M. Santos Carrião, A. Bakuzis, Mean-field and linear regime approach to magnetic hyperthermia of core-shell nanoparticles: can tiny nanostructures fight cancer? 8, 2016, pp. 8363–77.
- [16] C. Alexiou, R. Schmid, R. Jurgens, C. Bergemann, W. Arnold, F.G. Parak, Targeted tumor therapy with magnetic drug targeting: therapeutic efficacy of ferrofluid bond mitoxantrone, in: Stefan Odenbach (Ed.), *Ferrofluids: Magnetically Controllable Fluids and Their Applications*, Springer, 2002.
- [17] U. Maver, M. Bele, D. Makovec, S. Campbell, J. Jamnik, M. Gaberšček, Incorporation and release of drug into/from superparamagnetic iron oxide nanoparticles, *J. Magn. Magn. Mater.* 321 (19) (2009) 3187–3192.
- [18] R. Massart, Preparation of aqueous magnetic liquids in alkaline and acidic media, *IEEE Trans. Magn.* 17 (2) (1981) 1247–1248.
- [19] F.A. Tourinho, R. Franck, R. Massart, Aqueous ferrofluids based on manganese and cobalt ferrites, *J. Mater. Sci.* 25 (7) (1990) 3249–3254.
- [20] S.J. Iyengar, M. Joy, T. Maity, J. Chakraborty, R.K. Kotnala, S. Ghosh, Colloidal properties of water dispersible magnetite nanoparticles by photon correlation spectroscopy, *RSC Adv.* 6 (2016) 14393–14402.
- [21] S. Wiegand, T. Heinen, A. Ramaswamy, A. Sesterhenn, C. Bergemann, J. Werner, A. S. Lübbe, Evaluation of the tolerance and distribution of intravenously applied ferrofluid particles of 250 and 500 nm size in an animal model, *J. Drug Target.* 17 (3) (2009) 194–199.
- [22] S. Kückelhaus, V.A.P. Garcia, L.M. Lacava, R.B. Azevedo, Z.G.M. Lacava, E.C. D. Lima, F. Figueiredo, A.C. Tedesco, P.C. Morais, Biological investigation of a citrate-coated cobalt-ferrite-based magnetic fluid, *J. Appl. Phys.* 93 (10) (2003) 6707–6708. (<https://doi.org/10.1063/1.1558665>).
- [23] R.W. Chantrell, A. Bradbury, J. Popplewell, S.W. Charles, Agglomeration formation in a magnetic fluid, *J. Appl. Phys.* 53 (3) (1982) 2742.
- [24] A.F. Bakuzis, L.C. Branquinho, L.L. e Castro, M.T. de Amaral e Eloí, R. Miotti, Chain formation and aging process in biocompatible polydisperse ferrofluids: experimental investigation and monte carlo simulations, *Adv. Colloid Interface Sci.* 191–192 (2013) 1–21.
- [25] Z. Wang, C. Holm, Structure and magnetic properties of polydisperse ferrofluids: a molecular dynamics study, *Phys. Rev. E* 68 (2003), 041401. (<https://link.aps.org/doi/10.1103/PhysRevE.68.041401>).
- [26] C. Holm, A. Ivanov, S. Kantorovich, E. Pyanzina, E. Reznikov, Equilibrium properties of a bidisperse ferrofluid with chain aggregates: theory and computer simulations, *J. Phys.: Condens. Matter* 18 (38) (2006) S2737–S2756, <https://doi.org/10.1088/0953-8984/18/38/S14>.
- [27] A. Satoh, Application of the multi-particle collision dynamics method to a suspension of magnetic spherical particles, Vol. Volume 7: Fluids Engineering of ASME International Mechanical Engineering Congress and Exposition, 2017, v007T09A034. (<http://arxiv.org/abs/https://asmadigitalcollection.asme.org/IMECE/proceedings-pdf/IMECE2017/58424/V007T09A034/2500011/v007t09a034-imece2017-71184.pdf>), (<https://doi.org/10.1115/IMECE2017-71184>).
- [28] A.O. Ivanov, S.S. Kantorovich, Chain aggregate structure and magnetic birefringence in polydisperse ferrofluids, *Phys. Rev. E* 70 (2004), 021401. (<https://link.aps.org/doi/10.1103/PhysRevE.70.021401>).
- [29] A. Satoh, S.-I. Kamiyama, On aggregation phenomena in magnetic fluids by the tunnel theory and Monte Carlo simulations, *J. Colloid Interface Sci.* 172 (1995) 37.
- [30] A. Ghazali, J.-C. Levy, Two-dimensional arrangements of magnetic nanoparticles, *Phys. Rev. B* 67 (064409) (2003).
- [31] T. Kristóf, I. Szalai, Magnetic properties and structure of polydisperse ferrofluid models, *Phys. Rev. E* 68 (041109) (2003).
- [32] R. Weeber, M. Klinkigt, S. Kantorovich, C. Holm, Microstructure and magnetic properties of magnetic fluids consisting of shifted dipole particles under the influence of an external magnetic field, *J. Chem. Phys.* 139 (21) (2013), 214901, <https://doi.org/10.1063/1.4832239>.
- [33] E.L. Mackor, A theoretical approach of the colloid-chemical stability of dispersions in hydrocarbons, *J. Colloid Sci.* 6 (1951) 492–495.
- [34] R.E. Rosensweig, J.W. Nestor, R.S. Timmins, Ferrohydrodynamic fluids for direct conversion of heat energy, in: Proceedings of the Mater. Assoc. Direct Energy Convers. Proc. Symp. AlChE-I, vol. 5, 1965, 104.
- [35] T. Kruse, A. Spanoudaki, R. Pelster, Monte Carlo simulations of polydisperse ferrofluids: cluster formation and field-dependent microstructure, *Phys. Rev. B* 68 (054208) (2003).

- [36] L.L. Castro, M.F. daSilva, A.F. Bakuzis, R. Miotto, Aggregate formation on polydisperse ferrofluids: a Monte Carlo analysis, *J. Magn. Magn. Mater.* 293 (2005) 553.
- [37] L.L. Castro, R. Miotto, A.F. Bakuzis, Concentration effects on the grafting of magnetic nanoparticles by Monte Carlo simulations, *J. Appl. Phys.* 99 (08S101) (2006).
- [38] L.L. Castro, G.R.R. Gonçalves, K. Skeff, Neto, P.C. Morais, R. Miotto, Role of surfactant molecules in magnetic fluid: comparison of Monte Carlo simulation and electron magnetic resonance, *Phys. Rev. E* 78 (061507) (2008).
- [39] O. Schnitzer, M. Morozov, A generalized derjaguin approximation for electrical-double-layer interactions at arbitrary separations, *J. Chem. Phys.* 142 (24) (2015), 244102, <https://doi.org/10.1063/1.4922546>.
- [40] H.C. Hamaker, The London – van der waals attraction between spherical particles, *Physica* 4 (10) (1937) 1058.
- [41] G.M. Bell, G.C. Peterson, Calculation of the electric double-layer force between unlike spheres, vol. 41(3), 1972, pp. 542–66.
- [42] W.B. Russel, D.A. Saville, W.R. Schowalter, *Colloidal Dispersions*, Cambridge University Press, Cambridge; New York, 1989.
- [43] G.V. Lewis, C.R.A. Catlow, Potential models for ionic oxides, *J. Phys. C: Solid State Phys.* 18 (1985) 1149–1161. (<https://iopscience.iop.org/article/10.1088/0022-3719/18/6/010/meta>).
- [44] J. Israelachvili, *Intermolecular and Surface Forces*, Academic Press, Londres, 1992.
- [45] H. Ohshima, Electrophoretic mobility of a spherical colloidal particle in a salt-free medium, *J. Colloid Interface Sci.* 248 (2) (2002) 499–503, <https://doi.org/10.1006/jcis.2002.8232>.
- [46] D. Truzzolillo, F. Bordi, C. Cametti, S. Sennato, Counterion condensation of differently flexible polyelectrolytes in aqueous solutions in the dilute and semidilute regime, *Phys. Rev. E* 79 (2009), 011804, <https://doi.org/10.1103/PhysRevE.79.011804>.
- [47] D. Talbot, J. Queiros Campos, B.L. Checa-Fernandez, J.A. Marins, C. Lomenech, C. Hurel, G.D. Godeau, M. Raboisson-Michel, G. Verger-Dubois, L. Obeid, P. Kuzhir, A. Bee, Adsorption of organic dyes on magnetic iron oxide nanoparticles. Part I: mechanisms and adsorption-induced nanoparticle agglomeration, *ACS Omega* 6 (29) (2021) 19086–19098, <https://doi.org/10.1021/acsomega.1c02401>.
- [48] P.J. Flory, *Principles of Polymer Chemistry*, Cornell University Press, 1953.
- [49] D.F. Parsons, N. Eom, R.B. Walsh, V.S. Craig, A new divo-r theory: surface roughness and nanoparticle stability, in: *Harnessing Nanoscale Surface Interactions*, Elsevier, 2019, pp. 129–147.
- [50] W. Broer, G. Palasantzas, J. Knoester, V.B. Svetovoy, Roughness correction to the casimir force at short separations: contact distance and extreme value statistics, *Phys. Rev. B* 85 (15) (2012), 155410.
- [51] C. Genet, A. Lambrecht, P.M. Neto, S. Reynaud, The casimir force between rough metallic plates, *EPL (Europhys. Lett.)* 62 (4) (2003) 484.
- [52] R. Kodama, Magnetic nanoparticles, *J. Magn. Magn. Mater.* 200 (1–3) (1999) 359–372.
- [53] A.P. Caricato, A. Luches, Applications of the matrix-assisted pulsed laser evaporation method for the deposition of organic, biological and nanoparticle thin films: a review, *Appl. Phys. A* 105 (3) (2011) 565–582.
- [54] W. Thongswan, T. Kumpika, P. Singjai, Effect of high roughness on a long aging time of superhydrophilic TiO₂ nanoparticle thin films, *Curr. Appl. Phys.* 11 (5) (2011) 1237–1242.
- [55] Y. Zhang, D. Li, Y. Chen, Z. Li, A comparative study of ferrofluid seal and magnetorheological fluid seal, *IEEE Trans. Magn.* 54 (12) (2018) 1–7.
- [56] M.K. Hassanzadeh-Aghdam, M. Hasanzadeh, R. Ansari, Elastoplastic behavior of unidirectional hybrid composites containing SiO₂ nanoparticles under transverse tension, *Iran. J. Sci. Technol. Trans. Mech. Eng.* 44 (2) (2020) 299–312.
- [57] L. Reinert, I. Green, S. Gimmler, B. Lechthaler, F. Mücklich, S. Suárez, Tribological behavior of self-lubricating carbon nanoparticle reinforced metal matrix composites, *Wear* 408 (2018) 72–85.
- [58] N. Metropolis, A. Rosenbluth, M. Rosenbluth, A. Teller, E. Teller, Equation of state calculations by fast computing machines, *J. Chem. Phys.* 21 (1953) 1087.
- [59] W.K. Hastings, Monte Carlo sampling methods using Markov chains and their applications, *Biometrika* 57 (1) (1970) 97.
- [60] F.L.d.O. Paula, Saks analysis of magnetic field influence on magnetic nanoparticle clusters, *Condens. Matter* 4 (2) (2019). (<https://www.mdpi.com/2410-3896/4/2/55>).
- [61] I.I. Diakonov, Thermodynamic properties of iron oxides and hydroxides. II. estimation of the surface and bulk thermodynamic properties of ordered and disordered maghemite (γ -Fe₂O₃), *Eur. J. Mineral.* 10 (1) (1998) 17–30, <https://doi.org/10.1127/ejm/10/1/0017>.
- [62] M.L. Fdez-Gubieda, A. Garcí-Prieto, J. Alonso, C. Meneghini, X-Ray Absorption Fine Structure Spectroscopy in Fe Oxides and Oxyhydroxides, John Wiley & Sons, Ltd, 2016, pp. 397–422, <https://doi.org/10.1002/9783527691395.ch17>. Ch. 17.
- [63] M. Coduri, P. Masala, L. Del Bianco, F. Spizzo, D. Ceresoli, C. Castellano, S. Cappelli, C. Oliva, S. Checchia, M. Allietta, D.-V. Szabo, S. Schlabach, M. Hagelstein, C. Ferrero, M. Scavini, Local structure and magnetism of Fe₂O₃ maghemite nanocrystals: The role of crystal dimension, *Nanomaterials* 10 (5) (2020), <https://doi.org/10.3390/nano10050867>. (<https://www.mdpi.com/079-4991/10/5/867>).